J|A|C|S

A R T I C L E S

Direct Experimental Evaluation of Charge Scheme Performance by a Molecular Charge-Meter

Roie Yerushalmi,[†] Avigdor Scherz,*,[†] and Kim K. Baldridge[‡]

Contribution from the Department of Plant Sciences, The Weizmann Institute of Science, 76100 Rehovot, Israel, and the Department of Chemistry, University of California, San Diego, California 92093

Received November 11, 2003; E-mail: avigdor.scherz@weizmann.ac.il

Abstract: The remarkable advances accomplished in the past two decades in theoretical and computational capabilities have made the in silico study of complex chemical systems feasible. However, this progress is in strong contrast to the lag in experimental capabilities relating to the measurement of fundamental chemical quantities within convoluted environments such as solvents or protein milieu. As a result, many works rely extensively on predictions provided by ab initio methodologies without having independent experimental support. Such a proliferation of theory and computational approaches without being substantiated by appropriate experimental data is undesirable. The feasibility of using nickel−bacterio-chlorophyll as a *molecular potentiometer* was recently demonstrated for the systematic evaluation of fragmental charge density transfer for metal complexes in solution, thus providing an experimental assay with high accuracy and sensitivity (better than ±0.005 e⁻; Yerushalmi, R.; Baldridge, K. K.; Scherz, A. *J. Am. Chem. Soc.* **2003**, *125*, 12706−12707). Here the experimentally determined fragmental charge density transfer values measured by the molecular potentiometer for metal complexes in solvent are used to provide, for the first time, an independent and critical experimental evaluation of theoretical approaches commonly used in determining atomic charges and fragmental charge density transfer among interacting molecular systems. Importantly, these findings indicate that the natural population analysis (NPA) charge analysis is highly robust and well-suited for determining charge transfer processes involving donor−acceptor coordination interactions. The majority of computational charge schemes fail to provide an accurate chemical picture for the whole range of systems considered here. In cases where the role of electronic correlation varies significantly among chemically related structures, as with mono- and biligated complexes, the widely used electrostatic potential fit-based methods for evaluating atomic charges may prove to be problematic for predictive studies. In such cases, alternative methods that do not rely on the net dipole moment or other higher multipoles of the system for determining charges should be employed.

Introduction

Determination of charge distribution within and among chemical systems is central to the design and understanding of molecular systems. To deduce properties associated with charge distribution, one must exercise prior knowledge associated with the molecular system. Empirical approaches have been employed since the early days of modern chemistry to deduce indices such as electronegativity (χ) and hardness (η) that are associated with charge distribution between atoms in molecules. Such indices have provided considerable insight and are synonymous for chemical intuition. Yet, the quantitative utilization of these indices for complex and dynamic molecular systems is somewhat limited because of the strong need for specialized ad hoc parametrization required for specific systems and states. Still, at present, theoretical prediction of charge distribution and, in particular, fragmental charge density transfer among interacting chemical entities constitute some of the most basic properties pursued through modern quantum chemistry techniques. In particular, the concepts of atomic or group charges within a molecule are not uniquely defined within the quantum mechanical (QM) postulates;[1−4] therefore, the theoretical determination of "partial charge" is ambiguous and highly dependent on the specifics of the theoretical approach utilized.[5,6] This situation underscores the need for experimental approaches that enable direct evaluation of the theoretical results and that will provide the tools for further investigation of the basic concepts associated with the notion of partial charge. Although many literature studies have been done on the subject of charge distribution analyses,[3,7−12] even the most comprehensive ones

(1) Grier, D. L.; Streitwieser, A. *J. Am. Chem. Soc.* **1982**, *104*, 3556−3564.
(2) Bader, R. F. W. *Atoms in Molecules*, 1st paperback ed.; Clarendon Press: Oxford, U.K., 1994.
(3) Sigfridsson, E.; Ryde, U. *J. Comput. Chem.* **1998**, *19*, 377−395.
(4) Chermette, H. *J. Comput. Chem.* **1999**, *20*, 129−154.
(5) Bergman, D.; Hinze, J. *Angew. Chem., Int. Ed. Engl.* **1996**, *35*, 150−163.
(6) Wiberg, K. B.; Hadad, C. M.; Breneman, C. M.; Laidig, K. E.; Murcko, M. A.; LePage, T. J. *Science* **1991**, *252*, 1266−1272.
(7) Thompson, J. D.; Xidos, J. D.; Sonbuchner, T. M.; Cramer, C. J.; Truhlar, D. G. *PhysChemComm* **2002**, 117−134.
(8) Bultinck, P.; Langenaeker, W.; Lahorte, P.; De Proft, F.; Geerlings, P.; Waroquier, M.; Tollenaere, J. P. *J. Phys. Chem. A* **2002**, *106*, 7887−7894.
(9) Rousseau, B.; Peeters, A.; Van Alsenoy, C. *Chem. Phys. Lett.* **2000**, *324*, 189−194.

† Weizmann Institute of Science.
‡ University of California.

to date do not provide a sound experimental counterpart for reporting fragmental charges available by the variety of theoretical approaches and predictions. By nature, experimental monitoring of intra- and intermolecular fragmental charge density transfer extends beyond the computational objective.

Generally, bacteriochlorophylls (BChls) have been widely studied in the context of the broad range of functions that they perform in the photosynthetic light-harvesting and energy conversion machinery. These molecules operate as efficient antennas for harvesting light energy, as electron donors (e.g., BChl and [Zn]−BChl), and as electron acceptors (e.g., [H$_2$]−BChl). Progress in computational capabilities as well as ab initio methodologies has contributed to the better understanding of chlorophyll (Chl) and BChl's functions pertaining to light-harvesting and electron transfer processes.[13−18] This includes detailed studies of energy and electron distribution in intricate interacting systems containing several (B)Chl molecules (e.g., supramolecular forms) as well as the nearby amino acid residues.[18−21] During the past few years, we have developed and presented a novel approach that provides a means for an experimental look into sub-electron charge density transfer between metal centers and different ligands using metal-substituted bacteriochlorophylls ([M]−BChls).[22] In previous studies, we employed ab initio methodologies for complementing experimental techniques in the study of [M]−BChls' coordination chemistry, photochemistry, and electrochemistry, demonstrating their relevance as effective model systems for understanding enzymatic processes.[23−25] The [M]−BChl systems, and the [Ni]− and [Mn]−BChl systems, in particular, have proved to be versatile model systems for the study of elementary catalytic steps involving metal centers. In particular, we were able to track the dynamic role of charge mobilization and the mutual interplay of equatorial and axial ligands in various states of metal coordination.[23] As evident from these studies and others, careful application and interpretation of the data obtained by QM calculation techniques have enabled theoretical predictions of many of the important properties involved in chemical reactions. The rigorous QM study of these large molecular

(10) Kar, T.; Angyan, J. G.; Sannigrahi, A. B. *J. Phys. Chem. A* **2000**, *104*, 9953−9963.
(11) Rozas, I. *Int. J. Quantum Chem.* **1997**, *62*, 477−487.
(12) DeProft, F.; Martin, J. M. L.; Geerlings, P. *Chem. Phys. Lett.* **1996**, *250*, 393−401.
(13) Petke, J. D.; Maggiora, G. M.; Shipman, L. L.; Christoffersen, R. E. *Photochem. Photobiol.* **1980**, *32*, 399−414.
(14) Edwards, W. D.; Zerner, M. C. *Int. J. Quantum Chem.* **1983**, *23*, 1407−1432.
(15) Facelli, J. C. *J. Phys. Chem. B* **1998**, *102*, 2111−2116.
(16) Krueger, B. P.; Scholes, G. D.; Fleming, G. R. *J. Phys. Chem. B* **1998**, *102*, 5378−5386.
(17) Zhang, L. Y.; Friesner, R. A. *Proc. Natl. Acad. Sci. U.S.A.* **1998**, *95*, 13603−13605.
(18) Scholes, G. D.; Gould, I. R.; Cogdell, R. J.; Fleming, G. R. *J. Phys. Chem. B* **1999**, *103*, 2543−2553.
(19) Alden, R. G.; Parson, W. W.; Chu, Z. T.; Warshel, A. *Macroscopic and Microscopic Estimates of the Energetics of Charge Separation in Bacterial Reaction Centers*; Feldafing, Germany, 1995.
(20) Scherer, P. O. J.; Fischer, S. F. *Electronic Excitations and Electron-Transfer Coupling within the Bacterial Reaction Center Based on an INDO/S-CI Supermolecule Approach including 615 Atoms*; 1990; Vol. 22, pp 361−370.
(21) Lubitz, W.; Lendzian, F.; Bittl, R. *Acc. Chem. Res.* **2002**, *35*, 313−320.
(22) Yerushalmi, R.; Baldridge, K. K.; Scherz, A. *J. Am. Chem. Soc.* **2003**, *125*, 12706−12707.
(23) Yerushalmi, R.; Noy, D.; Baldridge, K. K.; Scherz, A. *J. Am. Chem. Soc.* **2002**, *124*, 8406−8415.
(24) Noy, D.; Yerushalmi, R.; Brumfeld, V.; Ashur, I.; Baldridge, K. K.; Scheer, H.; Scherz, A. *J. Am. Chem. Soc.* **2000**, *122*, 3937−3944.
(25) Ashur, I.; Brandis, A.; Greenwald, M.; Vakrat-Haglili, Y.; Rosenbach-Belkin, V.; Scheer, H.; Scherz, A. *J. Am. Chem. Soc.* **2003**, *125*, 8852−8861.

Scheme 1. [Ni]−BChl UV−Vis−NIR Absorption Spectra in Three States of Coordination with (A) No Axial Ligand, (B) One Axial Imidazole Ligand, and (C) Two Axial Imidazole Ligands[a]
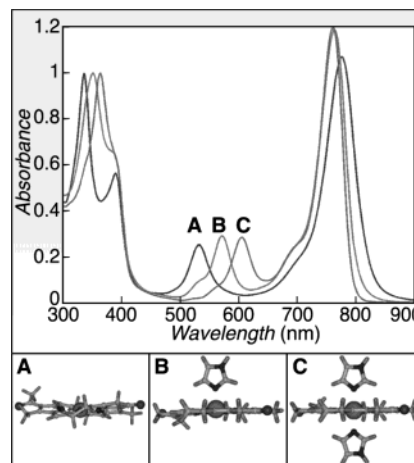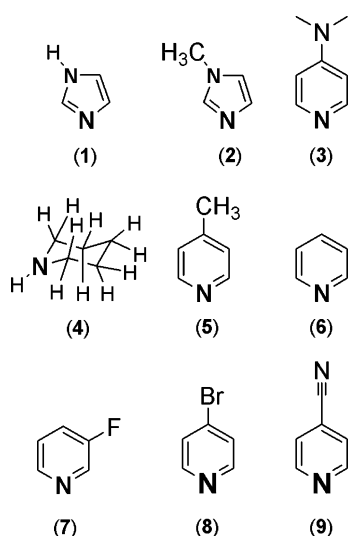

[a] Four electronic transition bands are observed: Q$_y$, Q$_x$, B$_x$, and B$_y$, in order of increasing energy. The ligand molecule is titrated at constant temperature, and the evolving spectra at each ligand concentration are recorded. The three components (A−C) are resolved using factor analysis techniques, providing the mole fraction (not shown) of each species and the ligation constants (K_{L1}^T and K_{L2}^T). Similarly, measuring the spectroscopic data for a constant ligand concentration at a range of temperatures provides the thermodynamic data [$\Delta G_{L1}^T(T, \Delta H_{L1}, \Delta S_{L1}), \Delta G_{L2}^T(T, \Delta H_{L2}, \Delta S_{L2})$].

systems, including transition metal atoms, has largely been made possible due to prudent application of efficient computational (hybrid) density functional theory (DFT), which reduces the exponential computational complexity of conventional electron correlation techniques, thus enabling affordable and efficient treatment of such important systems.

Recently,[22] we have shown that [Ni]−BChl can be used as an accurate and sensitive experimental assay, a "*molecular potentiometer*" for measuring fragmental charge density transfer. Comparison of the experimental results with independent QM calculations, performed for a series of compounds, showed that fragmental charge density transfer between the chelated metal center and reversibly bound ligand molecules can be accurately monitored experimentally, providing a counterpart for various computational and theoretical approaches. The molecular potentiometer is composed of a caged metal atom [Ni(II)] and a reduced tetrapyrrole bacteriopheophytin macrocycle (BPhe) that serves both as a chelator and as the "measuring device". The macrocycle of the [Ni]−BChl provides structural flexibility and a spectroscopic gauge (an asymmetric conjugated π system). The metal atom functions as a "probe" at the center that is capable of forming additional non-covalent binding interactions with small ligand molecules (Scheme 1). The axial ligand (D)/ [Ni]−BChl (A) complex may be regarded as a weakly interacting donor−acceptor system.

In the present study we have utilized the experimental data provided by the experimental assay for the independent, experimentally based evaluation of some of the most widely applied theoretical methodologies used for the prediction of charge distribution among molecular fragments. Herein we provide a concise description of selected charge analysis methodologies as specifically applied to the described molecular system. However, this work is not intended as an elaborate review, which can be found in degrees elsewhere.

Scheme 2. Ligand Molecules Used in the Present Study and the Abbreviations Used

Scheme 3. [Ni]−BChl *a* Molecule*a*

R=phytyl

a Peripheral positions were modified as schematically shown because of computational considerations.

For evaluation purposes, we report results obtained by several representative charge analysis schemes, including (a) electrostatic potential based methodologies (CHelpG[26] and MSK[27]) that employ fitting schemes under the constraint of reproducing the quantum chemical electrostatic potential as accurately as possible, (b) charges based on the atomic polar tensor analysis (APT),[28] (c) orbital-based methods (Mulliken population analysis),[29] and (d) density matrix based normal population analysis (natural population analysis, NPA).[30]

Materials and Methods

Chemicals. [Ni]−BChl was prepared according to the method of Hartwich et al.[31] Liquids were dried over activated molecular sieves (Sigma) according to the method of Burfield et al.,[32,33] degassed, and transferred under vacuum. Solid ligand molecules (Scheme 2) were of analytical grade from Aldrich and Sigma and used as received in freshly prepared 1 M acetonitrile (AN) solution.

Spectroscopic Titrations. Absorption spectra were recorded on a CARY 5 UV−visible−NIR spectrophotometer. Typically, 2 mL of a 5 μM [Ni]−BChl solution in dry AN was placed in a 10-mm optical pathway quartz cuvette that was sealed with a Teflon-coated rubber stopper. Ligands were injected through the septum with a gastight microliter syringe. A set of 10−15 spectra at different ligand concentrations was recorded during each titration. Ligand binding constants, the pure spectra of [Ni]−BChl at each coordination state, and their confidence intervals were derived from the spectra as previously described.[23,24]

Computational Methods. The QM study of systems that maintain the complexity and size considered here requires a careful balance of computational efficiency, on the one hand, and a rigorous treatment, on the other hand. On the basis of our previous experience in the study of [Ni]−BChl complexes, several modifications to the peripheral positions were introduced (Scheme 3) in order to facilitate the
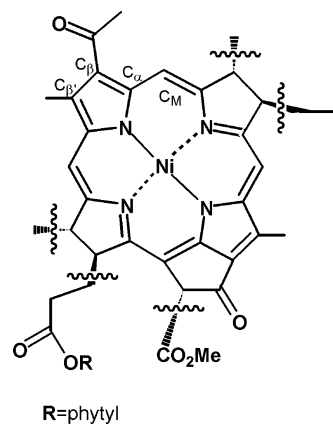
application of appropriate QM methodologies to the large array of structures considered here.

Such modifications do not introduce errors in the evaluation of properties studied here, particularly because we emphasize the *differences* between non-, mono-, and biaxially ligated structures.[23] In total, 17 structures were calculated at various levels of theory and charge analysis schemes, some with >1000 basis functions (fully optimized structures). In total, the equivalent of >20 CPU years (e.g., R12000, 400 MHz) were utilized to complete the computations, providing an excellent accumulation of data for the evaluation of behavior of the various levels of theory.

Geometry Optimization. The conformational analyses of the molecular systems described here, including structural and orbital arrangements as well as property calculations, were carried out by a variety of computational techniques for comparative purposes, using GAMESS[34] and GAUSSIAN 98.[35]

The scope of [Ni]−BChl systems addressed in the present study, including various states of coordination of relatively large molecular structures, offers relatively few basis set choices that will accommodate both the metal and the large size of the structure as well as incorporate the ability to adequately polarize and accommodate the angular momentum components of the metal. A particular difficulty associated with these systems involves finding a methodology that adequately represents the metal−nitrogen atom distances. The primary methodologies reported here include the hybrid density functional (HDFT) techniques,[36] which incorporate a portion of the exact Hartree−Fock exchange. We have considered several combinations of Becke's three-parameter hybrid exchange functional[37] with correlation functionals.

The correlation functionals include the widely used Lee−Yang−Parr (LYP) gradient-corrected correlation functional,[38] the Perdew and Wang 1991 functional[39] (PW91), and the Perdew 1986 functional

(26) Chirlian, L. E.; Francl, M. M. *J. Comput. Chem.* **1987**, *8*, 894−905.
(27) Besler, B. H.; Merz, K. M.; Kollman, P. A. *J. Comput. Chem.* **1990**, *11*, 431−439.
(28) Cioslowski, J. *J. Am. Chem. Soc.* **1989**, *111*, 8333−8336.
(29) Mulliken, R. S. *J. Chem. Phys.* **1955**, *23*, 1841−1846.
(30) Reed, A. E.; Curtiss, L. A.; Weinhold, F. *Chem. Rev.* **1988**, *88*, 899−926.
(31) Hartwich, G.; Fiedor, L.; Simonin, I.; Cmiel, E.; Schafer, W.; Noy, D.; Scherz, A.; Scheer, H. *J. Am. Chem. Soc.* **1998**, *120*, 3675−3683.
(32) Burfield, D. R.; Lee, K. H.; Smithers, R. H. *J. Org. Chem.* **1977**, *42*, 3060−3065.
(33) Burfield, D. R.; Smithers, R. H.; Tan, A. S. C. *J. Org. Chem.* **1981**, *46*, 629−631.
(34) Schmidt, M. W.; Baldridge, K. K.; Boatz, J. A.; Elbert, S. T.; Gordon, M. S.; Jensen, J. H.; Koseki, S.; Matsunaga, N.; Nguyen, K. A.; Su, S.; Windus, T. L.; Elbert, S. T. *J. Comput. Chem.* **1993**, *14*, 1347−1363.
(35) Frisch, M. J.; Trucks, G. W.; Schlegel, H. B.; Scuseria, G. E.; Robb, M. A.; Cheeseman, J. R.; Zakrzewski, V. G.; Montgomery, J. A. J.; Stratmann, R. E.; Burant, J. C.; Dapprich, S.; Millam, J. M.; Daniels, A. D.; Kudin, K. N.; Strain, M. C.; Farkas, O.; Tomasi, J.; Barone, V.; Cossi, M.; Cammi, R.; Mennucci, B.; Pomelli, C.; Adamo, C.; Clifford, S.; Ochterski, J.; Petersson, G. A.; Ayala, P. Y.; Cui, Q.; Morokuma, K.; Malick, D. K.; Rabuck, A. D.; Raghavachari, K.; Foresman, J. B.; Cioslowski, J.; Ortiz, J. V.; Stefanov, B. B.; Liu, G.; Liashenko, A.; Piskorz, P.; Komaromi, I.; Gomperts, R.; Martin, R. L.; Fox, D. J.; Keith, T.; Al-Laham, M. A.; Peng, C. Y.; Nanayakkara, A.; Gonzalez, C.; Challacombe, M.; Gill, P. M. W.; Johnson, B.; Chen, W.; Wong, M. W.; Andres, J. L.; Gonzalez, C.; Head-Gordon, M.; Replogle, E. S.; Pople, J. A. *GAUSSIAN 98*, revision A.6 ed.; Gaussian, Inc.: Pittsburgh, PA, 1998.
(36) Parr, R. G.; Yang, W. *Density Functional Theory of Atoms and Molecules*; New York, 1989.
(37) Becke, A. D. *J. Chem. Phys.* **1993**, *98*, 5648−5652.
(38) Lee, C.; Yang, W.; Parr, R. G. *Phys. Rev.* **1988**, *B37*, 785−789.
(39) Perdew, J. P.; Wang, Y. *Phys. Rev. B* **1992**, *45*, 13244−13249.

(P86).[40] These HDFT functionals were considered with three basis sets that employ relativistic effective core potentials (RECPs) on the heavy atoms:

(1) The Los Alamos National Laboratory 2-double-ζ (LANL2DZ),[41,42] treats explicitly the valence and "valence-1" shells, as indicated by the "2".

(2) The Stuttgart and Dresden (SDD) basis set incorporates single f functions for Ni and, as well, employs the double-ζ valence basis set of Dunning on the first- and second-row atoms.

Both the LANL2DZ and SDD basis sets are of double-ζ quality in the valence and "valence-1" shells, whereas the RECP contains Darwin and mass−velocity contributions of Hay and Wadt[41,43,44] in the former case [note, for Ni this is (5s,5p,5d) → [3s,3p,2d]] and of Stuttgart and Dresden in the latter [note, for Ni this is (8s7p6d1f) → [6s5p3d1f]].

These RECP have been determined to be a computationally very efficient and reliable approaches for handling relativistic effects, which must be accounted for in the complexes involving nickel.[45]

(3) The triple-ζ quality basis set combination (TZV) employs the 6-311G(d,p) basis set for the first- and second-row elements and the Ahlrich TZV basis set for heavy atoms.[46]

The nature of each stationary point was uniquely characterized by calculating and diagonalizing the matrix of energy second derivatives (Hessian) to determine the number of imaginary frequencies (0 = minima; 1 = transition state). In cases where structures with multiple imaginary frequencies were located, we followed the corresponding vibrational eigenvector modes for location of the global minimum.

Atomic Charge Analyses. Atomic charges were derived by means of various charge schemes and at a range of levels of theory for comparative purposes. In particular, we considered the Mulliken population analysis (Mull), the least-squares fit to the electrostatic potential (ESP) according to the ChelpG and Merz−Singh−Kollman (MSK) schemes,[27,47] the NPA,[30,48] and the atomic polar tensor based (APT) analysis.[28]

To obtain good numerical accuracy, the MSK scheme incorporated a large number of points chosen on nested Connolly surfaces with a density of 1 point/Å, sampling points at 1.4, 1.6, 1.8, and 2.0 times the van der Waals (vdW) radius of the atoms. The APT analysis was performed using an auxiliary program provided by Martin JML.[49]

To provide a systematic evaluation of the electron correlation contribution on population analysis, we have performed a set of single-point computations at the same reference geometry that has been evaluated at the optimal level of theory (HDFT/basis) as described in the section above. We include in this evaluation Hartree−Fock (HF), second-order Møller−Plesset perturbation theory (MP2), and HDFT densities.

In particular, the NPA was performed for all complexes at the following levels of theory: (1) HF/LANL2DZ//B3LYP/LANL2DZ; (2) B3LYP/LANL2DZ; (3) HF/SDD//B3P86/SDD; (4) B3P86/SDD; and (5) MP2/SDD// B3P86/SDD.

Additionally, the following levels of theory were considered with the [Ni]−BChl·(**6**)$_1$ and [Ni]−BChl·(**6**)$_2$ complexes for evaluating the behavior of the mono- and biligated structures: (6) B3LYP/SDD and (7) B3P86/LANL2DZ.

MP2 single points were carried out using the fully direct algorithm as implemented in the GAUSSIAN 98 suite of software, running on an Itanium cluster housing 20 GB of fast memory.

(40) Perdew, J. P. *Phys. Rev. B* **1986**, *33*, 8822−8824.
(41) Hay, P. J.; Wadt, W. R. *J. Chem. Phys.* **1985**, *82*, 299−310.
(42) Dunning, T. H., Jr.; Hay, P. J. *Modern Theoretical Chemistry*; Plenum: New York, 1976.
(43) Hay, P. J.; Wadt, W. R. *J. Chem. Phys.* **1985**, *82*, 270−283.
(44) Wadt, W. R.; Hay, P. J. *J. Chem. Phys.* **1985**, *82*, 284−298.
(45) Siegbahn, P. E. M. *Adv. Chem. Phys.* **1996**, *93*, 333−387.
(46) Schafer, A.; Horn, H.; Ahlrichs, R. *J. Chem. Phys.* **1992**, *97*, 2571−2577.
(47) Singh, U. C.; Kollman, P. A. *J. Comput. Chem.* **1984**, *5*, 129−145.
(48) Reed, A. E.; Weinstock, R. B.; Weinhold, F. *J. Chem. Phys.* **1985**, *83*, 735−746.
(49) Martin, J. M. L.; Van Alsenoy, C. *GAR2PED, a Gaussian Output Postprocessing Utility*; University of Antwerp: Antwerp, Belgium, 1995.

Results and Discussion

Experimental Results. As shown in Scheme 1, the evolving spectra could be resolved to three spectroscopic components, corresponding to the absorption spectra of the non-, mono-, and biaxially ligated complexes. In two cases, however, the spectroscopic titrations with ligand molecules **8** and **9** showed only the biligated species [[Ni]−BChl·(**8**)$_2$ and [Ni]−BChl·(**9**)$_2$]. Thus, in total, seven titrations provided three spectroscopic components each, and two titrations provided two spectroscopic components each, with characteristic spectroscopic bands (Q$_y$, Q$_x$, B$_x$, and B$_y$ in order of increasing energy). The resolved spectroscopic data are presented in Table 1 of ref 1 and are depicted here for the clarity of discussion.

Interestingly, the ligand molecules **7**−**9** have the lowest gas basicity values among the ligands used in this study: 870.1, 886.0, and 848.8 kJ/mol, respectively.[50] For axial coordination to the Ni(II) metal center, the high-spin ground state ($S = 1$) electronic configuration is energetically favored compared with the low-spin ($S = 0$) state. In contrast, for the nonligated structure, the high-spin state is substantially higher in energy compared with the low-spin ground state in the gas phase. Thus, the single addition of a weak axial ligand is energetically unfavorable. However, the geminal addition of two axial ligand molecules, when present in high concentrations to produce the high-spin hexacoordinated complex, is energetically favored even in cases of weak ligand molecules such as **8** and **9**, because the total energy released upon the binding of two ligand molecules is sufficiently high in these cases. It should be noted that in such cases where the change in free energy associated with the axial ligand binding process is *not* highly exothermic, the overall energetic balance is determined by the solvation energy and the solvent coordination properties, for example, ligand molecule **7,** which has a gas basicity value of 870.1 kJ/mol, somewhat lower than the corresponding value for ligand molecule **8**, yet the monoligated species is observed in solution.

Comparison of the experimental charge transfer values ($\Delta Q_{\mathrm{M}}^{\circ}$, Table 1) for ligand molecules **1**−**7**, where both mono- and biaxially ligated complexes are observed, reveals that upon second axial ligand binding the amount of charge transferred by each ligand molecule is significantly decreased (with an average of 12 ± 2.5% per single ligand molecule) compared with the amount transferred in the corresponding monoligated complex.

Q$_x$ Band Shift. The amount of charge at the [M]−BChl metal center can be determined quantitatively by the spectroscopic band shifts.[23,24,51] Specifically, $\Delta Q_{\mathrm{M}}^{\circ}$ involves a linear combination of the Q$_y$ and Q$_x$ bands shifts (ΔEQ_x and ΔEQ_y). The value, ΔEQ_y, primarily results from changes in the effective radius of the metal because of metal substitution[51] and core expansion induced by reversible binding of axial ligand molecules to a metal center.[23,24] In the latter case, for a particular metal center, such as Ni(II) studied here, the change in the effective radius of the metal results primarily from the change involved in going from a geometrically contracted Ni(II) low-spin ($S = 0$) configuration to the expanded core of the Ni(II) high-spin ($S = 1$) state.[22] The data obtained for the set of 16 complexes show that the amount of charge transfer, $\Delta Q_{\mathrm{M}}^{\circ}$,

(50) Hunter, E. P. L.; Lias, S. G. *J. Phys. Chem. Ref. Data* **1998**, *27*, 413−656.
(51) Noy, D.; Fiedor, L.; Hartwich, G.; Scheer, H.; Scherz, A. *J. Am. Chem. Soc.* **1998**, *120*, 3684−3693.

Table 1. Spectroscopic Energy Band Shifts of Mono- and Biaxially Ligated Complexes of [Ni]−BChl Relative to the Nonligated Molecule in AN[a]

complex[b]	spectroscopic band shifts (eV)				charge transfer
	$-\Delta EB_y$	$-\Delta EB_x$	$-\Delta EQ_x$	$-\Delta EQ_y$	$-\Delta Q_M^\circ$ (e⁻)
[Ni]−BChl·$(\mathbf{1})_1$	0.1574	0.0000	0.1585	−0.0309	0.2977
[Ni]−BChl·$(\mathbf{2})_1$	0.1189	0.0000	0.1587	−0.0252	0.2948
[Ni]−BChl·$(\mathbf{3})_1$	0.1381	0.0000	0.1565	−0.0272	0.2928
[Ni]−BChl·$(\mathbf{4})_1$	0.1357	0.0000	0.1565	−0.0281	0.2920
[Ni]−BChl·$(\mathbf{5})_1$	0.1123	0.0000	0.1452	−0.0295	0.2672
[Ni]−BChl·$(\mathbf{6})_1$	0.1543	0.0000	0.1404	−0.0334	0.2630
[Ni]−BChl·$(\mathbf{7})_1$	0.1437	0.0000	0.1316	−0.0438	0.2400
[Ni]−BChl·$(\mathbf{1})_2$	0.2769	0.0000	0.2774	−0.0354	0.5305
[Ni]−BChl·$(\mathbf{2})_2$	0.2806	0.0000	0.2729	−0.0321	0.5246
[Ni]−BChl·$(\mathbf{3})_2$	0.2799	0.0000	0.2677	−0.0342	0.5139
[Ni]−BChl·$(\mathbf{4})_2$	0.2659	0.0000	0.2643	−0.0334	0.5059
[Ni]−BChl·$(\mathbf{5})_2$	0.2712	0.0000	0.2488	−0.0347	0.4779
[Ni]−BChl·$(\mathbf{6})_2$	0.2676	0.0000	0.2471	−0.0354	0.4739
[Ni]−BChl·$(\mathbf{8})_2$	0.2686	0.0000	0.2355	−0.0330	0.4541
[Ni]−BChl·$(\mathbf{7})_2$	0.2740	0.0000	0.2299	−0.0349	0.4437
[Ni]−BChl·$(\mathbf{9})_2$	0.2236	0.0000	0.2247	−0.0305	0.4286

[a] [Ni]−BChl·$(\mathbf{m})_n$, where $\mathbf{m} = 1-9$ corresponds to the specific ligand molecule as shown in Scheme 2, and $n = 1, 2$ corresponds to mono- and biaxially ligated complexes, respectively. Charge-transfer values, ΔQ_M°, were determined from the spectroscopic band shifts according to the method of Noy et al.[51] [a] Data reproduced from ref 22.

which contains contributions from both the Q_x and Q_y band shifts, correlates nicely with ΔEQ_x as a *single* experimental observable:[22]

$$\Delta Q_M^\circ = a \times \Delta EQ_x + b \tag{1}$$

In eq 1, a and b are the linear fit parameters, $R^2 = 0.99$.

As previously noted, the constant shift, b, prominently reflects the expansion of the metal center upon axial ligation. For the rest of the discussion that follows, we make use of ΔEQ_x as a direct measure for the amount of charge transferred to the metal center. It is interesting to note that the measured amount of charge density transfer (using the values of ΔQ_M°, or ΔEQ_x) for a series of related ligand molecules agrees with the order of corresponding group electronegativity values. Specifically, the amount of charge density transfer measured for ligand molecules **3** and **5**−**9**, where the pyridine residue was systematically substituted, follows the order $NMe_2 > CH_3 > H > Br > F >$

CN. These observations are further supported by the excellent correlation with ab initio results (vide infra) as shown below.

Computational Results. The linear correlation given in eq 1[22] encouraged us to perform a thorough QM study for the purpose of obtaining an independent theoretical characterization of the Q_x band response, as a result of charge transfer induced by the reversible bonding of axial ligand molecules. Tables 2 and 3 show the computational results, from which selected results are illustrated and compared to experimental data in Figures 1 and 2 for clarity and in the following discussion. Computational charge transfer values (ΔN_{Lig}) for the [Ni]−BChl·$(\mathbf{m})_n$ complexes were obtained by summation of the atomic charge values for the atoms of the axial ligand fragment of the corresponding mono- or biligated complex, obtained by each charge scheme. The x coordinate of the graphs depicted in these figures corresponds to the amount of calculated charge, ΔN_{Lig}, transferred by the axial ligand(s) using various computational charge analysis schemes. The y coordinate represents the spectroscopic band shift, ΔEQ_x, which is directly related to the amount of the experimentally determined charge transfer, ΔQ_M°. Panels a and b of Figure 2 show the computational result versus ΔEQ_x for the structures calculated at the B3P86/SDD and B3LYP/LANL2DZ levels of theory, respectively.

Although it is well-established that ab initio quantum chemical calculations coupled with adequate basis set descriptions for small- and medium-sized molecules typically yield accurate structures and electronic properties, large molecular structures, especially those containing transition metals such as metalloporphyrins, often require particular care in computational treatments in order to be useful for quantitative predictions. This situation is demonstrated in the present study results, where similar chemical structures of mono- and biligated [Ni]−BChl complexes show diverse patterns of behavior. The addition of polarization functions has a significant effect, especially for the properties of biligated complexes, whereas the properties of monoligated complexes show much less variability. For example, the calculated charge transfer in the [Ni]−BChl·$(\mathbf{6})_1$ and [Ni]−BChl·$(\mathbf{6})_2$ complexes increases when using the SDD basis set as compared to the LANL2DZ basis set by 7.6 and 27.9%, respectively, with the B3LYP functional and by 5.4 and 28.0%,

Table 2. Computational Results of Charge Transfer between Axial Ligand(s) and the [Ni]−BChl Molecule[a]

complex	B3P86/SDD					/MP2/SDD//	HF//	B3P86/LNL
	ΔN_{Lig} NPA (e⁻)	ΔN_{Lig} Mulliken (e⁻)	ΔN_{Lig} ESP (e⁻)	ΔN_{Lig} ChelpG (e⁻)	ΔN_{Lig} APT (e⁻)	ΔN_{Lig} NPA (e⁻)	ΔN_{Lig} NPA (e⁻)	ΔN_{Lig} NPA (e⁻)
[Ni]−BChl·$(\mathbf{1})_1$	0.1204	0.1707	0.2258	0.1969	0.1572	0.0944	0.0751	
[Ni]−BChl·$(\mathbf{2})_1$	0.1223	0.1855	0.2287	0.2042	0.1637	0.0991	0.0752	
[Ni]−BChl·$(\mathbf{3})_1$	0.1215	0.1994	0.2127	0.1930	0.1622	0.0957	0.0691	
[Ni]−BChl·$(\mathbf{4})_1$	0.1355	0.2771	0.1954	0.1598	0.1274	0.0929	0.0657	
[Ni]−BChl·$(\mathbf{5})_1$	0.1106	0.1799	0.1922	0.1644	0.1496	0.0860	0.0636	
[Ni]−BChl·$(\mathbf{6})_1$	0.1105	0.1680	0.1841	0.1572	0.1452	0.0877	0.0650	0.1048
[Ni]−BChl·$(\mathbf{7})_1$	0.1036	0.1461	0.1602	0.1416	0.1276	0.0830	0.0634	
[Ni]−BChl·$(\mathbf{1})_2$	0.2303	0.1219	0.7342	0.1667	0.2023	0.2098	0.1646	
[Ni]−BChl·$(\mathbf{2})_2$	0.2318	0.1644	1.0346	0.1411	0.2088	0.2107	0.1642	
[Ni]−BChl·$(\mathbf{3})_2$	0.2241	0.1315	1.4377	0.2426	0.1780	0.1979	0.1516	
[Ni]−BChl·$(\mathbf{4})_2$	0.2227	0.3926	0.5291	−0.0179	0.0997	0.1760	0.1248	
[Ni]−BChl·$(\mathbf{5})_2$	0.2137	0.1126	1.0623	0.2717	0.1647	0.1898	0.1465	
[Ni]−BChl·$(\mathbf{6})_2$	0.2115	0.0879	1.4760	0.2921	0.1623	0.1889	0.1461	0.1652
[Ni]−BChl·$(\mathbf{8})_2$	0.2039	0.0675	1.5557	0.3248	0.1199	0.1831	0.1434	
[Ni]−BChl·$(\mathbf{7})_2$	0.2000	0.0453	1.3389	0.2676	0.1262	0.1796	0.1413	
[Ni]−BChl·$(\mathbf{9})_2$	0.1975	0.0518	1.1839	0.2476	0.1116	0.1760	0.1414	

[a] Molecular structures calculated using the B3P86 functional with the LANL2DZ and SDD basis sets, as indicated, and the subsequent charge analysis performed according to the particular methodology specified.

Table 3. Computational Results of Charge Transfer between Axial Ligand(s) and the [Ni]−BChl Molecule[a]

	B3LYP/LNL					HF/LNL//	B3LYP/SDD
complex	ΔN_{Lig} NPA (e−)	ΔN_{Lig} Mulliken (e−)	ΔN_{Lig} ESP (e−)	ΔN_{Lig} ChelpG (e−)	ΔN_{Lig} APT (e−)	ΔN_{Lig} NPA (e−)	ΔN_{Lig} NPA (e−)
[Ni]−BChl·(**1**)$_1$	0.1064	0.2340	0.2351	0.1987	0.1379	0.0244	
[Ni]−BChl·(**2**)$_1$	0.1095	0.2493	0.2337	0.2059	0.1438	0.0525	
[Ni]−BChl·(**3**)$_1$	0.1111	0.2641	0.2231	0.2041	0.1418	0.0200	
[Ni]−BChl·(**4**)$_1$	0.1262	0.3129	0.2181	0.1773	0.1243	0.0442	
[Ni]−BChl·(**5**)$_1$	0.1020	0.2456	0.2042	0.1763	0.1311	0.0175	
[Ni]−BChl·(**6**)$_1$	0.0998	0.2342	0.1963	0.1691	0.1268	0.0169	0.1073
[Ni]−BChl·(**7**)$_1$	0.0925	0.2175	0.1802	0.1515	0.1058	0.0153	
[Ni]−BChl·(**1**)$_2$	0.1677	0.4514	0.7238	0.1915	0.1645	0.0655	
[Ni]−BChl·(**2**)$_2$	0.1711	0.4792	0.6725	0.1296	0.1737	0.0698	
[Ni]−BChl·(**3**)$_2$	0.1654	0.4851	1.3213	0.2635	0.1356	0.0535	
[Ni]−BChl·(**4**)$_2$	0.1738	0.5802	0.4909	−0.0412	0.0837	0.0386	
[Ni]−BChl·(**5**)$_2$	0.1555	0.4568	1.0971	0.1579	0.1256	0.0480	
[Ni]−BChl·(**6**)$_2$	0.1523	0.4385	1.3471	0.2846	0.1231	0.1251	0.1948
[Ni]−BChl·(**8**)$_2$	0.1459	0.4167	1.1988	0.2298	0.0804	0.0436	
[Ni]−BChl·(**7**)$_2$	0.1421	0.4051	1.2738	0.1836	0.0866	0.0421	
[Ni]−BChl·(**9**)$_2$	0.1394	0.4029	0.9557	0.2054	0.0615	0.0698	

[a] Molecular structures calculated using the B3LYP functional with the LANL2DZ and SDD basis sets, as indicated, and the subsequent charge analysis performed according to the particular methodology specified.
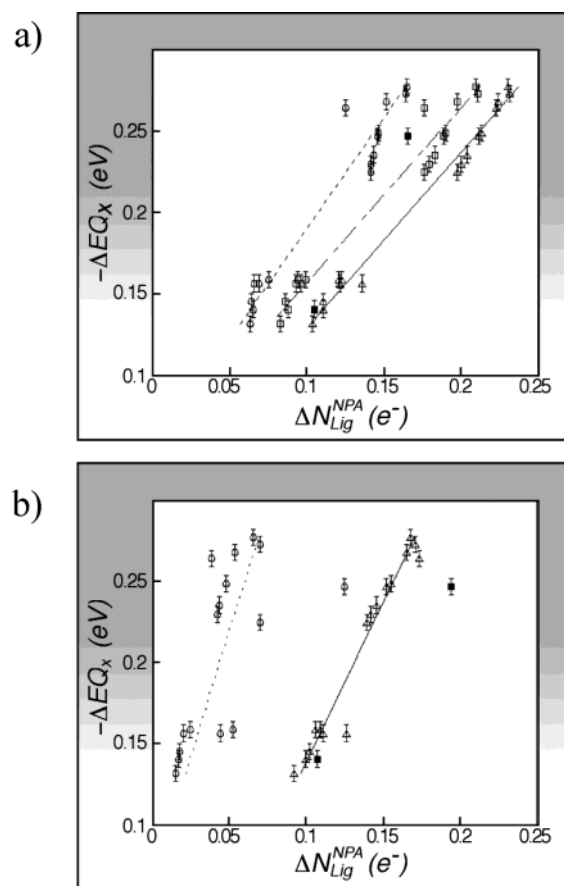

Figure 1. Measured Q$_x$ band shift of [Ni]−BChl·(**m**)$_n$ complexes relative to the [Ni]−BChl molecule in AN versus the calculated charge transferred using the NPA scheme. Structures were calculated at the (a) B3P86/SDD and (b) B3LYP/LANL2DZ levels of theory. The charge analysis was performed using the HDFT (△), MP2 (□), and HF densities (○). The [Ni]−BChl·(**6**)$_{1,2}$ complexes (■) are shown at the (a) B3P86/LANL2DZ and (b) B3LYP/SDD levels of theory as well.

Figure 2. Measured Q$_x$ band shift of [Ni]−BChl·(**m**)$_n$ complexes relative to the [Ni]−BChl molecule in AN versus the calculated charge transferred with the Mulliken (○), MKS (□), ChelpG (△), and APT (×) schemes. The structures were calculated and analyzed at the (a) B3P86/SDD and (b) B3LYP/LANL2DZ levels of theory.

respectively, when using the B3P86 functional (Tables 2 and 3). This nonhomogeneous behavior for the biligated complexes is also expressed in other electronic parameters that are discussed in the following sections.
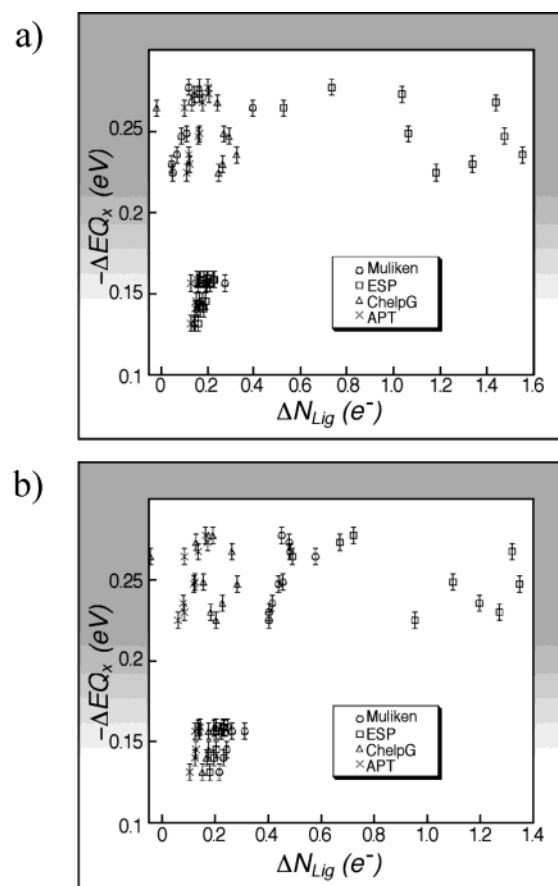
Among the various levels of theory considered here, we find that the B3P86/SDD is by far more consistent with the experimental charge transfer data across the full set than any of the others. This result is in line with other studies where the B3P86 functional was shown to provide accurate results for molecules that encompass transition metal atoms, and in several cases results even superior to those of the rather popular B3LYP

functional were obtained.[52–56] One such study that is particularly worth noting is a comparative study performed for $3d$ transition metals, where it was observed for homonuclear Ni molecules that the B3P86 functional was the *only* (H)DFT functional to converge to the correct electronic configuration.[57]

The excellent linear correlation found for ΔEQ_x and the calculated charge transfer, ΔN_{Lig}^{NPA} ($R^2 = 0.99$ for the NPA analysis, B3P86/SDD), is in line with the experimental observation shown above that the value of ΔEQ_x can be used as a *single* experimental observable for determining the amount of charge transferred by the axial ligand(s) to the Ni(II) metal center.[22] Thus, we use the spectroscopic band shift as a gauge for determining the fragmental charge density transfer between the [Ni]–BChl and axial ligand(s).

The sizable difference between the empirically (ΔQ_M°) and computationally derived charge density transfer (ΔN_{Lig}^{NPA}) reflects experimental parameters and level of theory used in the frame of the experimental model and QM calculations, respectively. Specifically, the empirical model relies on the transformation of the observed spectroscopic changes as a result of variations in the metal's electronegativity and effective radius to charge units.[31] Additionally, within that model, the electronic density is estimated by considering point charges, rather than the full charge density distribution. Importantly, such parametrizations do not affect the linear correlation with the spectroscopic response to perturbations in the charge density, but rather lead to changes in scaling of the absolute values in terms of elementary charge units.

Furthermore, even when comparing a variety of ab initio methodologies with the same charge analysis scheme, one obtains different "slopes" for the correlation of computationally derived charges because of the noncompleteness of the particular QM methods. For example, using different HDFT functionals with the same basis set (SDD) and charge analysis (e.g. NPA), one obtains different slopes for linear correlations among the computational schemes (e.g., 0.90 for B3LYP/SDD vs B3P86/SDD).

As such, one may expect a priori that comparison of ΔQ_M° values with results obtained by ab initio QM methods would require scaling factors. Therefore, the linear correlation found for ΔEQ_x and ΔN_{Lig}^{NPA} is of profound importance because it enables the direct translation of the observed changes in a single experimental observable to charge density expressed in elementary charge units.

This experimental gauge offers exceptional sensitivity and accuracy, as evident from the quality of the linear correlation with ab initio results (Figure 1a and Table 4) and the small experimental error limits (± 0.005 e$^-$). This approach of using a spectroscopic probe without the need to crystallize or introduce other drastic perturbations to the measured molecular systems (such as an electrode interface) allows one to look at the fine details of charge transfer processes between axial ligands and

Table 4. Correlation Coefficients (R^2) of Linear Fits across Experimental (Q$_x$ and ΔQ_M°) and Theoretical Charge Analysis (NPA) Using the HF, MP2, and HDFT Densities[a]

	ΔQ_M°	ΔEQ_x	NPA HF	NPA MP2	NPA HDFT
ΔQ_M°		**0.99(9)**	**0.94**/*0.41*	**0.97**/-	**0.99**/*0.96*
ΔEQ_x			**0.94**/*0.41*	**0.97**/-	**0.99**/*0.96*
NPA HF				0.99/-	0.95/*0.38*
NPA MP2					0.98/-
NPA HDFT					

[a] Comparison with experimental data shown in bold font. Geometries obtained at the B3P86/SDD level of theory (normal font) and at the B3LYP/LANL2DZ level of theory (italics).

transition metals in solution. In particular, we investigated the role of electron correlation on the predictions for the charge transfer process. Figure 1a shows the change in charge units and quality of linear fit as a result of choosing various electron correlation treatments. Results obtained using the HF, MP2, and the HDFT (B3P86) densities are presented. Charge analysis was performed at the same reference geometry for comparison. Overall, the agreement with the experimental results follows the same order (HF < MP2 < HDFT). A detailed investigation of the results shows that although the physicochemical behaviors of the mono- and biligated complexes are similar, the latter (the upper right data points set in Figure 1) shows a much higher tendency to disperse from the linear correlation with experimental data when electron correlation treatment beyond the HF level is excluded. This tendency reflects the fact that the biligated complexes [[Ni]–BChl·(**m**)$_2$] are of the donor–acceptor–donor (D–A–D) type, whereas the monoligated complexes [[Ni]–BChl·(**m**)$_1$] are of the donor–acceptor (D–A) type. The former pose a challenge for ab initio methodologies. Unlike the D–A case where electrostatic interactions are dominant, in the D–A–D case, there is a much smaller net dipole moment [e.g., 2.03 and 8.52 D for [Ni]–BChl·(**3**)$_2$ and [Ni]–BChl·(**3**)$_1$, respectively], with substantial push–pull interactions for which electron correlation has a significant contribution.

Additional indications of the variant nature of the D–A–D complexes, as compared to the D–A complexes, was extracted from calculations that show substantial effects of adding polarization functions to the Ni atom, in the case of biligated (D–A–D) complexes, whereas for the monoligated (D–A) complexes, such effects are much smaller. Such an example is shown in Figure 1 (solid rectangle) for the [Ni]–BChl·(**6**)$_1$ and [Ni]–BChl·(**6**)$_2$ complexes. Although only a moderate dependency on polarization functionality is observed for the monoligated complex, a substantial effect (~28%) is observed when one shifts from the LANL2DZ basis set to the SDD basis set for the biligated complex, for both the B3LYP and B3P86 functionals. In light of these observations, the NPA performance is remarkable, because it provides a homogeneous description for both the mono- and biligated complexes when compared with the experimental data set. Furthermore, the NPA results are well-behaved in the sense that improvement of the basis set and electron correlation treatment results in excellent agreement with the experimental data (Table 4).

Performance of Various Charge Analysis Schemes. The possibility of accurately following fragmental charge density transfer in the [Ni]–BChl·(**m**)$_n$ system offers a unique experimental tool for evaluating the performance of many of the widely used charge analysis schemes. Such an experimental tool

(52) Triguero, L.; Wahlgren, U.; Pettersson, L. G. M.; Siegbahn, P. *Theor. Chim. Acta* **1996**, *94*, 297−310.
(53) Godbout, N.; Havlin, R.; Salzmann, R.; Debrunner, P. G.; Oldfield, E. *J. Phys. Chem. A* **1998**, *102*, 2342−2350.
(54) BelBruno, J. J. *Heteroatom Chem.* **1998**, *9*, 651−657.
(55) Wiener, J. J. M.; Politzer, P. *J. Mol. Struct. (THEOCHEM)* **1998**, *427*, 171−174.
(56) Bosnick, K. A.; Haslett, T. L.; Fedrigo, S.; Moskovits, M.; Chan, W. T.; Fournier, R. *J. Chem. Phys.* **1999**, *111*, 8867−8870.
(57) Barden, C. J.; Rienstra-Kiracofe, J. C.; Schaefer, H. F. *J. Chem. Phys.* **2000**, *113*, 690−700.

Table 5. Correlation Coefficients (R^2) of Linear Fits across Experimental (ΔEQ_x) and Theoretical Charge Analysis Schemes (NPA, ESP, ChelpG, APT, and Mulliken) Using the HDFT Densities[a]

	ΔEQ_x	NPA	ESP	ChelpG	APT	MULL
	(A) All 16 Complexes Studied					
ΔEQ_x		**0.99/0.96**	**0.62/0.60**	**0.02/0.01**	**0.08/0.00**	**0.03/0.91**
NPA			0.67/0.48	0.03/0.03	0.04/0.00	0.05/0.96
ESP				0.39/0.14	0.00/0.09	0.37/0.49
ChelpG					0.01/0.03	0.74/0.08
APT						0.04/0.03
MULL						
	(B) Monoligated Species [Ni]−BChl·(**1**−**7**)$_1$, excluding [Ni]−BChl·(**4**)$_1$					
ΔEQ_x		**0.97/0.92**	**0.98/0.98**	**0.98/0.98**	**0.93/0.90**	**0.60/0.50**
NPA			0.94/0.84	0.98/0.97	0.93/0.95	0.63/0.76
ESP				0.98/0.94	0.90/0.84	0.51/0.38
ChelpG					0.89/0.92	0.55/0.61
APT						0.80/0.69
MULL						

[a] Comparison with the experimental data shown in bold font. Geometries and densities obtained at the B3P86/SDD level of theory (normal font) and at the B3LYP/LANL2DZ level of theory (italics).

enables one to look at charge transfer processes involving a transition metal center with various ligand molecules. As shown in the previous section, the Q_x band shift provides an accurate experimental gauge that can be used as a reference for comparing the computational results (Table 4, $R^2 = 0.99$).

We considered several representative charge analysis schemes of diverse algorithmic types, including the well-known orbital-based Mulliken population analysis method,[29] charges based on the atomic polar tensor analysis (APT),[28] and the electrostatic-potential based methodologies, ChelpG[26] and MSK.[27]

For the ligand molecules that demonstrate both mono- and biligated complexes, the amount of charge transferred by the second axial ligand over that of the first, as measured by the molecular potentiometer,[22,23] is lower compared with the corresponding monoligated complex with the respective ligand molecule. This experimental observation is readily understood by the fact that the metal center becomes partly saturated by the charge transferred by the first axial ligand. As we illustrated in the previous section, the NPA reproduces this behavior with high fidelity, despite the fact that the electrostatic characteristics of the complexes considered are very diverse. Although this may be straightforward from the experimentalist's point of view, we recognize that the majority of computational charge schemes (except for NPA) fail to give the correct chemical picture for the whole range of systems considered here. However, a meticulous examination of the computational results shows that most charge schemes provide good to excellent correlation with experimental data for the subset of monoligated complexes, with the exception of the Mulliken analysis, which performs relatively poorly (Table 5B), as might be expected. Furthermore, the addition of polarization functions (here via the SDD basis set) produces computational results obtained by the various charge analysis schemes for the monoligated complexes that are much more consistent among the set, as compared to the less polarized (LANL2DZ) basis set (for a comparison, see the lower left data points in Figure 2a,b). In the following sections we will elaborate on these findings according to details of the respective charge analysis methodology.

Mulliken Charges. Mulliken charge analysis was historically one of the first QM methodologies used for deriving atomic charges and is still widely used today. This method is typically

a standard output generated by many QM software tools, and many studies actually include the Mulliken charge analysis in some way. However, this method suffers from several acute deficiencies that are well-documented in the literature, as noted by Mulliken.[58] The prominent limitation of this method is that it usually provides chemically meaningless results due to the fact that it partitions the overlapping densities in a relatively arbitrary manner. Additionally, results are highly dependent on the choice of basis set functions. Our results support these observations quantitatively and qualitatively, as can be seen in Table 5 and Figure 2, respectively. Quantitatively, the correlation coefficients, obtained for ΔN_{Lig} for Mulliken charge analysis with either ΔEQ_x or NPA results for the whole data set, are highly irregular ($R^2 = 0.03$ for B3P86/SDD and 0.91 for B3LYP/LANL2DZ vs ΔEQ_x) with the better fit obtained for the lower level of theory (also a well-established phenomenon). Consideration of the qualitative features of the data reveals that the Mulliken analysis at the higher level of theory (B3P86/SDD) predicts the total amount of charge transferred by two axial ligands to be less than the amount transferred by the corresponding single axial ligand (Figure 2a), a phenomenon known to be incorrect. When the performance for the set of monoligated complexes is exclusively considered, the correlation coefficients for both the B3P86/SDD and B3LYP/LANL2DZ levels of theory are similarly inadequate for the data shown.

Atomic Polar Tensor Charges. Cioslowski's APT charge analysis is based on dipole moment derivatives that can be related to experimental observables.[12,28] However, this method is not extensively applied due to the relatively high computational demand, especially when large molecular systems containing unsaturated bonds are studied. Moreover, the APT scheme is relatively sensitive to electron correlation effects;[12,28] therefore, it requires a higher level of theory for a reliable determination of atomic charges. To the best of our knowledge, the present work is the most extensive study to date in which the APT analysis is applied to relatively large transition metal complexes in a systematic manner, across various levels of theory.

Our results indicate that with regard to the entire data set, including the biligated complexes, the APT analysis predictions at the highest level of theory currently feasible for complexes of the size considered here are still quite poor (Table 5A). However, when only the monoligated complexes are considered, the APT analysis predictions are relatively good, especially for the more polarized basis set (Table 5B). This phenomenon may be explained by the fact that electron correlation effects are more dominant in the D−A−D systems than in the D−A systems. Thus, it may be interesting to consider the biligated systems at higher levels of theory, provided that adequate computational means are feasible.

Electrostatic Fit-Based Charges. Among the most widely used methods for the prediction of atomic charges are various schemes of least-squares fit to the electrostatic potential obtained from QM methods. The various schemes diverge, on the basis of the particular method of choosing the points in space for which the electrostatic potential is calculated. Because there are a large variety of available methods, we considered the prevalent MSK and ChelpG schemes. The MSK scheme establishes points on nested Connolly surfaces and sample points at 1.4, 1.6, 1.8,

(58) Politzer, P.; Mulliken, R. S. *J. Chem. Phys.* **1971**, *55*, 5135−5136.

and 2.0 times vdW radius of the associated atoms. The ChelpG scheme points are selected on the basis of a regularly spaced cubic grid and include points that are external to the vdW radius of atoms up to a distance of 2.8 Å (vdW $< r <$ vdW $+ 2.8$ Å).

Interestingly, both schemes show excellent performance with no substantial dependency on the level of theory for the monoligated D−A polar complexes ($R^2 = 0.98$, Table 5B). However, for the entire data set, including the substantially less polar D−A−D biligated complexes, performance is degraded almost completely. This phenomenon can be better understood if one realizes that most electrostatic potential-based charge methods are based on what the molecule "feels" as the probe charge approaches. Such methods have the most problems in assigning charge values associated with atoms buried within the molecular framework and away from the external surface. This is the case in the D−A−D complexes where the metal center, A, is in its highest coordination capacity, "solvated" with the axial ligands as well as the four nitrogens of the BChl macrocycle chelator. This is clearly the result of choosing points to fit external to the vdW radius or coinciding volumes of adjacent atoms. As such, any sort of scheme for the electrostatic fit of atomic charge would be deficient, because, due to axial symmetry, the net dipole moment of the D−A−D systems is much smaller than that of the corresponding D−A systems. Additionally, charge transfer in the D−A−D systems has an appreciable contribution due to electron correlation effects that are not necessarily expressed in the electrostatic potential outside the vdW radius or easily represented by a fit of the electrostatic surface.

Concluding Remarks

We have investigated and demonstrated the ambiguity involved in the determination of atomic charges by means of various computational techniques. As such, we have been able to identify failures of various methodologies as well as to provide insight as to their origin, utilizing an accurate experimental benchmark. Our results indicate that, for charge distributions in systems that involve transition metal complexes, unless an adequate level of theory is employed, neither conventional nor hybrid density functional methodologies are useful for the prediction of properties associated with electron transfer processes. Moreover, once the adequate QM methodology is established, the subsequent charge analysis scheme employed must be critically evaluated.

Our findings indicate that the NPA charge analysis is highly robust and is well-behaved for determining charge transfer processes involving donor−acceptor coordination interactions. The NPA results are monotonically improved when a more complete basis set is applied, along with post-HF electron correlation treatments. This behavior was not observed for any of the other schemes considered in this work, throughout the complete set of complexes studied. The proper choice of HDFT

functional has proven to deliver superior results at an affordable computational cost, even when compared to computationally intensive correlation approaches, such as MP2 theory. However, one must bear in mind that functional-based methods, such as offered by density functional theory, involve parametrization of both the exchange and correlation functionals, which affect their performance according to the training set originally used to do such a parametrization. In cases when the role of electronic correlation varies significantly among chemically related structures, as in the present study, the widely used electrostatic potential fit-based methods for evaluating atomic charge may prove to be problematic for predictive studies. In such cases, methods that do not rely on the net dipole moment or other higher multipoles of the system for determining charges should be employed. This conclusion is cardinal for the fruitful application of QM methodologies in the study of metalloproteins, which have become more commonly the subject of investigation in recent years due to the availability of very capable computing infrastructures, as well as the development of efficient software for large molecular systems.

In the present approach we have demonstrated a protocol for devising specialized molecular systems as "molecular tools" for the study of fundamental chemical and physical phenomena, which has been presented as a proof-of-principle. When these particular molecular constructs are considered as tools, an important engineering aspect emerges for a modular design strategy, made possible by means of the various functional sites naturally present in the BChl macrocycle. Recent progress in BChl-related chemical modifications initiated in our group and by others has enabled us to tailor the desired properties and functional characteristics for further generalization of the possible application of these structures as tools. In particular, metal incorporation into the (B)Chl macrocycle (with M = Pd, Zn, Ni, Cd, Cu, Mn, Co, and, more recently, Pt, Hg, and Fe), combined with macrocycle peripheral modification, enables a rational, stepwise design of molecules with specialized photophysical, photochemical, and coordination properties as well as their application for monitoring microscopic details of various environments.